PAPER Nr. : 40

EFFECTS OF ROTATING FRAME TURBULENCE AND DYNAMIC STALL ON GUST RESPONSE OF HELICOPTER BLADES

BY

R. MADHAVAN AND G.H. GAONKAR

FLORIDA ATLANTIC UNIVERSITY
DEPT. OF MECHANICAL ENGINEERING
BOCA RATON, FLORIDA, USA

FIFTEENTH EUROPEAN ROTORCRAFT FORUM

SEPTEMBER 12 - 15, 1989 AMSTERDAM

Effects of Rotating Frame Turbulence and Dynamic Stall on Gust Response of Helicopter Blades

R. Madhavan and G.H. Gaonkar

Abstract

Rotating frame turbulence, or RFT, refers to the actual turbulence experienced by the blades and requires noneulerian description and sampling of measurements. Its characteristics are strikingly different from those of conventional models based on eulerian or space-fixed turbulence description, and these differences increase with decreasing advance ratio and altitude. For example, in axial flight, though the RFT and space-fixed turbulence are stationary, the RFT spectral density shows large peaks at the integer multiples of the rotor speed (1P, 2P etc.) and transfer of energy essentially from the low-frequency region ($\leq$ 1P) to the high-frequency region ($>$ 1P). These characteristics cannot be predicted by the space-fixed description and severely affect helicopter gust-response statistics. In forward flight, the differences in characteristics are much more fundamental in that the RFT becomes nonstationary, though the space-fixed turbulence remains stationary. This paper presents the instantaneous or frequency-time spectrum of RFT, which provides a means of predicting the transfer of energy with respect to frequencies and the periodically varying nonstationarity with respect to time. It also presents the RFT effects on the response statistics of an isolated rotor blade for low-advance-ratio and low-altitude conditions. The blade is modeled to include flap bending degrees of freedom and dynamic stall effects.

Introduction

In the presence of turbulence, the flight dynamics requirements of helicopters are becoming increasingly demanding. Typical examples include NOE maneuvers, lighthouse and offshore oil-platform missions and ship landing (Refs.1-3). Turbulence also affects the flight dynamics of other air vehicles that combine the hovering efficiency of

helicopters with the cruising efficiency of airplanes (Refs.4,5). The tilt rotor "chugging" problem, which is basically a fore-to-aft low-frequency acceleration of the rigid body mode coupling with the rotor torque mode, is a case in point. It occurs at relatively low speeds of about 150 knots and aggravates during descent (Ref.5). This has prompted a greater appreciation of turbulence modeling, particularly at low altitudes and advance ratios, and of turbulence effects on low-frequency response and stability, pilot's work load and flight control systems (Refs.1,6-8). Concerning helicopter structural dynamics, significant strides have been made toward understanding turbulence effects on fatigue, ride quality and vibrations (Refs.4,9-11).

Modeling Turbulence

Turbulence is typically modeled on the assumption that it is uniform over the rotor disk. This means that turbulence as experienced at the hub center is a representative sample of the entire disk and that the conventional eulerian or space-fixed description of turbulence is satisfactory (Refs.4,11). Therefore, as is done in airplanes, the turbulence excitation at a blade station can be directly represented by the eulerian-description models such as those of Dryden and von Karman. In fact, an earlier study (Ref.11), with reference to high-speed compound helicopters (advance ratio μ=1.6), compared the eulerian description with the more accurate noneulerian or rotating frame turbulence (RFT) description and concluded that RFT effects are negligible. It must be emphasized that Ref.11 neglects the effects of airflow velocity in the axial direction on the turbulence correlation distance. For such high-speed conditions ($\mu \simeq$1.6), the correlation distance is virtually determined by the dominant flight speed with negligible contributions from the rotational and axial-flow velocities. In sharp contrast to this finding of negligible RFT effects, extensive investigations of wind turbines have shown dominant RFT effects on turbulence characteristics and turbine response (Refs.12,13).

Recently, Ref.14 presents a generalized RFT model that is valid in axial as well as forward flight. On the basis of RFT characteristics, it qualitatively explains the two contrasting findings of negligible RFT effects for high-speed flights (μ >0.8) and

dominant RFT effects on wind turbines. For μ <0.4, the characteristics of RFT are strikingly different from those of space-fixed turbulence, and these differences are sensitive to frequencies and increase with decreasing advance ratio (Ref.14). However, in Ref.14, this frequency sensitivity treatment is restricted to the stationary hovering conditions, and the conventional spectral density description used therein is not applicable to the nonstationary forward-flight conditions. A follow-up study, Ref.3, demonstrates the appreciable RFT effects on low-frequency flight dynamics response in hover, including corroboration by the GENHEL flight dynamics simulation program. As shown in Ref.3, RFT effects on response increase with decreasing values of turbulence scale length L. It is emphasized that L decreases with decreasing altitude, and near obstacles, L has values comparable to the rotor radius R. This paper introduces the instantaneous or frequency-time spectral density of RFT, which provides a means of simultaneously predicting the frequency sensitivity in the frequency domain and the periodically varying nonstationarity in the time domain, as required in forward flight. It also investigates the RFT effects on rotor response in forward flight, with emphasis on low-advance-ratio and low-altitude conditions. To put this paper in proper perspective, it is expedient to review first the characteristics of RFT vis-a-vis space-fixed turbulence, including experimental validation.

RFT Studies

Experimental and analytical investigations of RFT effects on wind turbines are fairly extensive (e.g. Refs.12,13). Fig. 1 from Ref.13 includes the predicted spectral density of the longitudinal or fore-to-aft turbulence velocity at a blade station according to the von Karman model. Some minor quantitative differences between the actual Bessel function model used in Ref.13 and the von Karman Bessel function model are bypassed here. The fore-to-aft component, perpendicular to the turbine plane, is the most dominant component, as is the axial or vertical component for rotorcraft. To capture the RFT effects, the data base was generated from the noneulerian sampling of measurements along a circular array of points that represent the instantaneous loci of

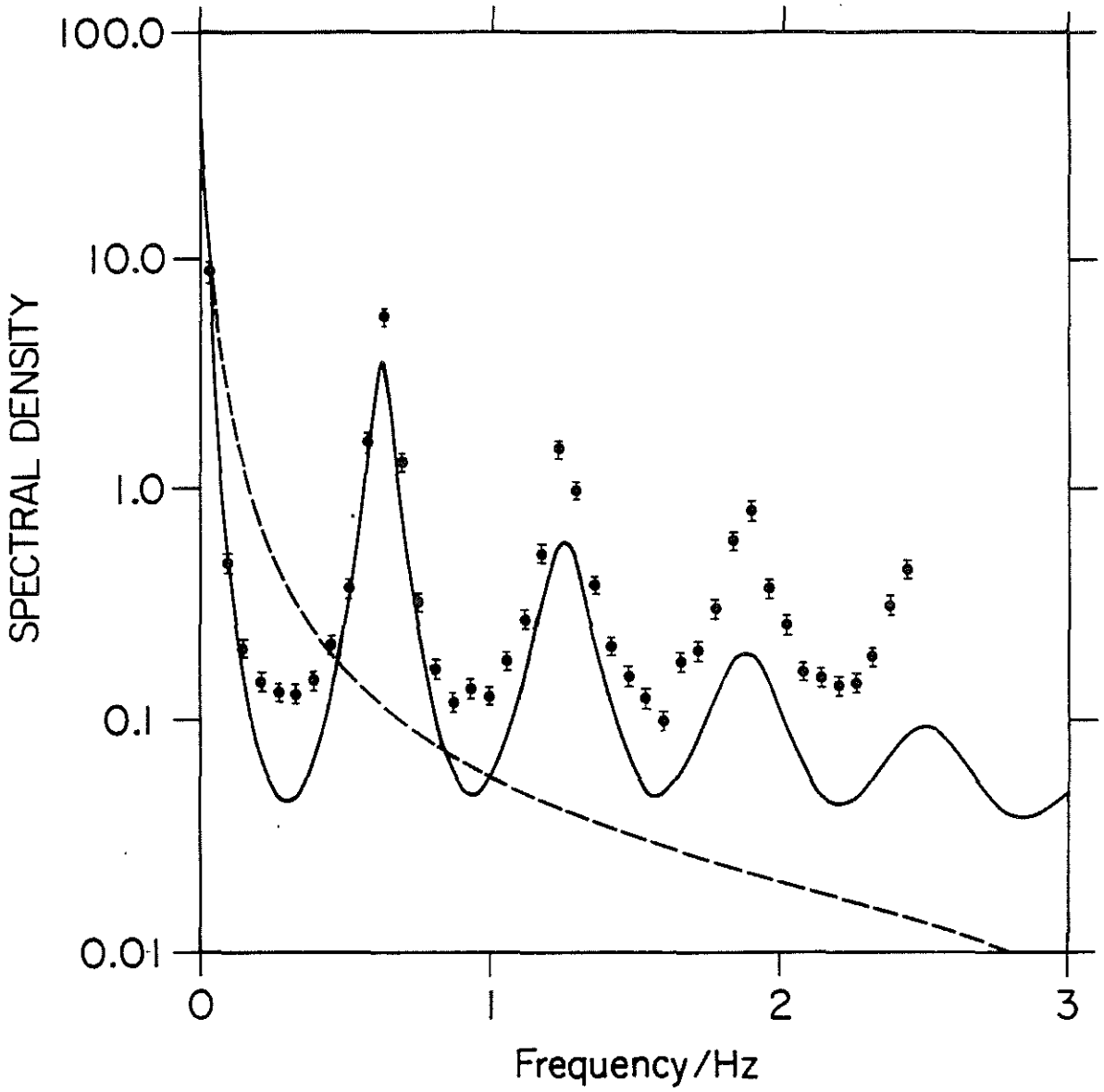

Figure 1 Spectrum of longitudinal wind speed fluctuations, as seen from a rotating blade station (RFT), compared with the space-fixed spectrum (Ŧ Experiment,— von Karman with RFT,--- von Karman without RFT)

this station (For details, see Refs.12 and 13). The monotonically decaying behaviour is exhibited by the conventional eulerian description, which fails to capture the two basic features of data: transfer of energy from the essentially low-frequency region (<1P; P: rotational speed) to the higher-than-1P region and the occurrence of peaks at 1P, 2P etc. By comparison, the RFT description dramatically improves the correlation. The correlation also shows that the assumptions of isotropy, homogeneity and momentarily frozen wave field are fairly valid. The overall validity of the Taylor-von Karman theory of free atmospheric turbulence is indeed remarkable, given the complexities at low altitudes such as earth's boundary layer, closeness to obstacles and low values of turbulence scale length. Similarly, the spectral density S(f) of the vertical turbulence velocity at the 0.7R blade station is shown in Fig. 2 on the basis of the Dryden model, which is widely used in flight-dynamics studies. The results are presented as f*S(f) versus ln f, which gives a better picture of the spectral density variation or transfer of energy in the low-frequency region. It is noteworthy that the area under the curve $\int fS(f)d(\ln f)$ gives the variance, as in the conventional S(f)-versus-f presentation shown in the upper-left inset figure. The upper-right inset figure refers to the autocovariance function $R(\tau)$. Since the area under the spectral density curve is the same in both the space-fixed and rotating-frame description, the transfer of energy from the low-frequency (<1P) region to the high-frequency ($\geq$1P) region is balanced by the occurrence of peaks. The RFT effects of transfer of energy and occurrence of peaks cannot be captured in the space-fixed description of turbulence modeling.

Turbulence Modeling

Following Ref.14, a brief account of turbulence modeling is given here to facilitate the subsequent discussion of numerical results. So that RFT may be better appreciated without being masked by the complexities of the turbulence flow field, only the dominant vertical turbulence velocity w(t) at one blade station, say 0.7R from the centre, is considered. An additional feature not covered earlier includes the instantaneous spectral density $S_w(f,t)$, which shows the distribution of the mean square value ("energy")

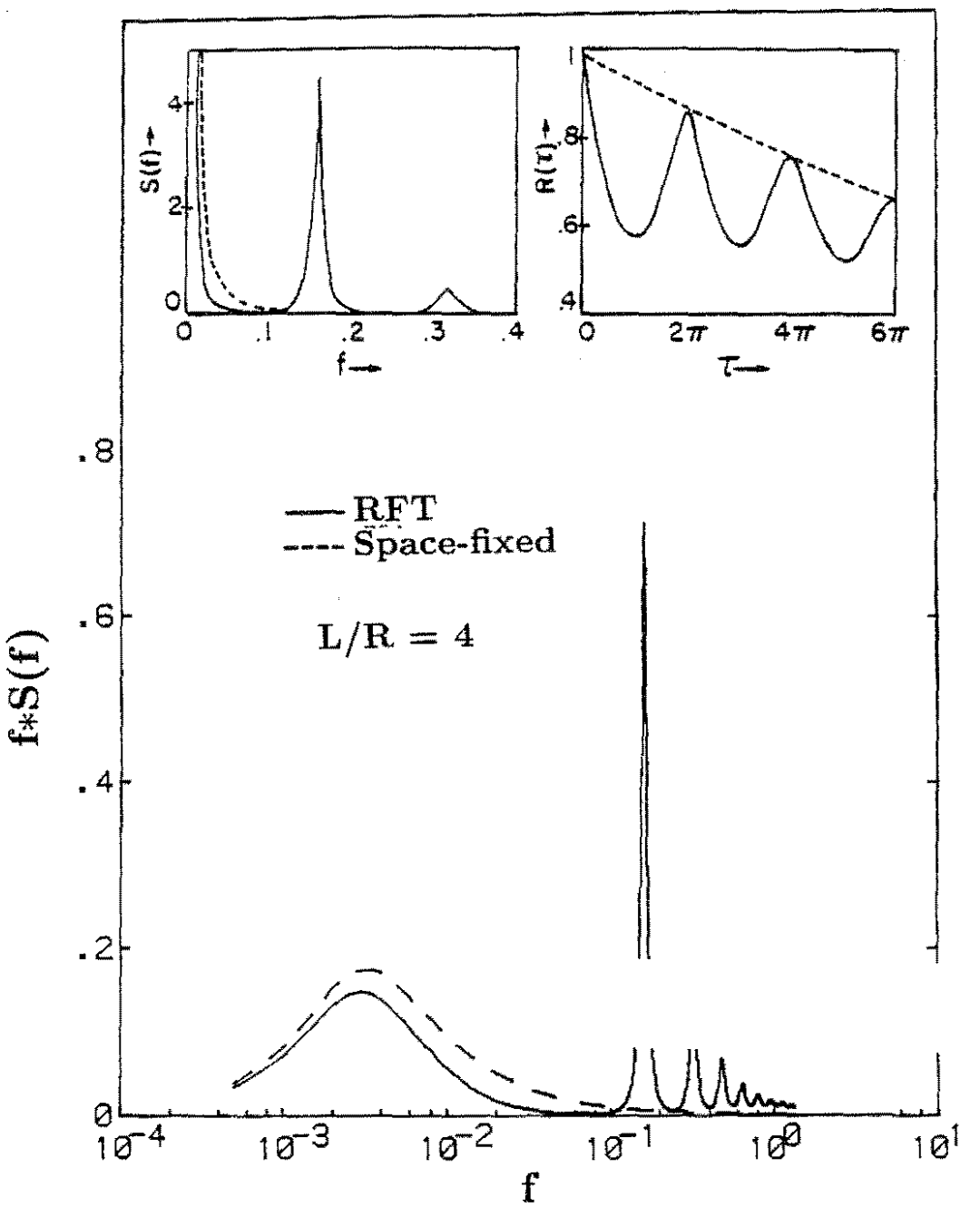

Fig.2 RFT Effects on Space-fixed Dryden Model for the vertical turbulence at 0.7R blade station.

in the f-t or frequency-time domain. The $S_w(f,t)$ in combination with its autocovariance function $R_w(\tau,t)$ provides a physically complete picture of RFT regarding both energy transfer from the low-frequency region to the high-frequency region and its periodically varying nonstationary structure. Referring to the rotor-fixed xyz system as typified in Fig. 3, the instantaneous flow velocity components are

$$\frac{dx}{dt} = V + 0.7\Omega R \sin\Omega t \tag{1a}$$

$$\frac{dy}{dt} = V + 0.7\Omega R \cos\Omega t \tag{1b}$$

$$\frac{dz}{dt} = U \tag{1c}$$

where U is the total mean flow in the z or plunge direction perpendicular to the disk (opposite of shaft direction) due to flight speed and mean turbulence flow including downwash. From the Taylor - von Karman theory, the autocovariance funtion $R_w(t_1,t_2)$ can be expressed as a function of the spatial correlation distance r, which is $\{r(t_2)-r(t_1)\}$, and the spatial coordinates quantifying r can be converted into temporal coordinates t_1 and t_2. Thus,

$$r = \left[\{X(t_2)-X(t_1)\}^2 + \{Y(t_2)-Y(t_1)\}^2 + \{Z(t_2)-Z(t_1)\}^2\right]^{\frac{1}{2}} \tag{2a}$$

$$R_w(t_1,t_2) = \sigma_w^2 g(r) \tag{2b}$$

where σ_w is the rms value or intensity of vertical turbulence. The form of g(r) depends upon the model adopted. For example, in the von Karman model, g(r) involves algebraically cumbersome Bessel functions. The present treatment uses Dryden and much simpler exponential models, which are good approximations to the von Karman model in the low-frequency region. For the exponential model,

$$R_w(t_1,t_2) = \sigma_w^2 e^{-|r|/(L/2)} \tag{3}$$

where L/2 is the turbulence scale length of the vertical turbulence velocity. With the following notations,

$$\frac{V\cos\alpha}{\Omega R(L/2)R} = \frac{\mu}{(L/2)R} = \frac{2\mu}{(L/R)} = a,$$

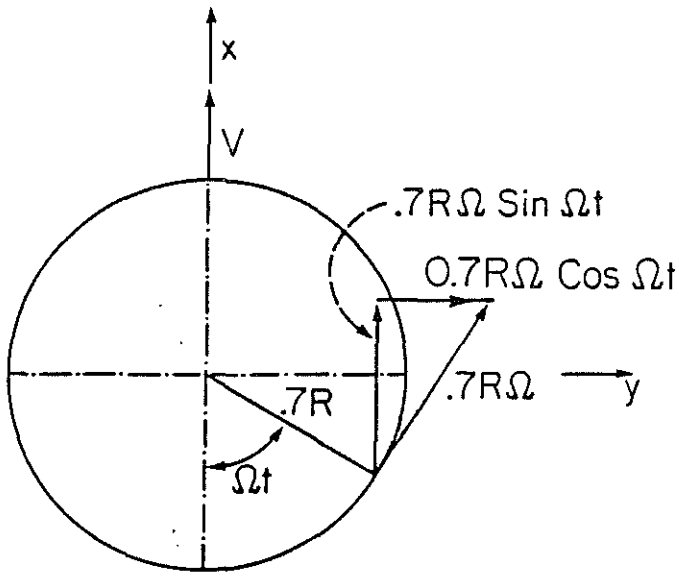

Fig.3 Rotor in Forward Flight (Momentum theory)

r in equation(2a) can be expressed as

$$\begin{aligned}\frac{r}{(L/2)} &= [\{a(\bar{t}_2-\bar{t}_1)-1.4\,(R/L)\cos\bar{t}_2+1.4\,(R/L)\cos\bar{t}_1\}^2 \\ &\quad +\{1.4\,(R/L)\sin\bar{t}_2-1.4\,(R/L)\sin\bar{t}_1\}^2 \\ &\quad +\{2\overline{U}\,(R/L)\,(\bar{t}_2-\bar{t}_1)\}^2]^{\frac{1}{2}} \end{aligned} \tag{4}$$

where

$$\bar{t}_1=\Omega t_1,\quad \bar{t}_2=\Omega t_2,\quad \overline{w}=w/\Omega R,\quad \overline{U}=U/\Omega R$$

To better understand the stochastic structure of the RFT characteristics, it is convenient to use the following temporal coordinates:

$$\bar{t}_2-\bar{t}_1=\tau,\qquad \frac{(\bar{t}_1+\bar{t}_2)}{2}=t$$

and the following notations:

$$b=(R/(L/2))\,\overline{U}\quad and\quad c=0.7R/(L/2)$$

Now the autocovariance function $R_w(t,\tau)$ takes the form

$$R_w(t,\tau)=\sigma_w^2 exp\left[-\{\tau^2(a^2+b^2)+4c\sin\tau/2(c\sin\tau/2+a\tau\sin t)\}^{\frac{1}{2}}\right] \tag{5}$$

Observe that

$$R_w(t+2m\pi,\tau+2n\pi)=R_w(t,\tau)\quad only\quad for\quad m=n \tag{6}$$

and thus the process is periodically stationary. However, it must be emphasized that the process is not mean square periodic since equation (6) does not hold for m≠n, nor is it (weakly) stationary since equation (5) is not a function of τ only. Fig. 4 shows $R_w(t,\tau)$ typified by equation (5). The assumed parameter values are identified in the figure and are typical of low-altitude (say, L/R≃5) conditions. The periodic structure of nonstationarity along the t-axis and the dominant RFT effects at low advance ratios (μ <0.2) are noteworthy, and as expected, the RFT effects decrease with increasing values of μ and L/R. In hover a=0, and equation (5) simplifies to

$$R_w(t,\tau)=R_w(\tau)=\sigma_w^2 exp\left[-\{\tau^2b^2+4c^2\sin^2\tau/2\}^{\frac{1}{2}}\right] \tag{7a}$$

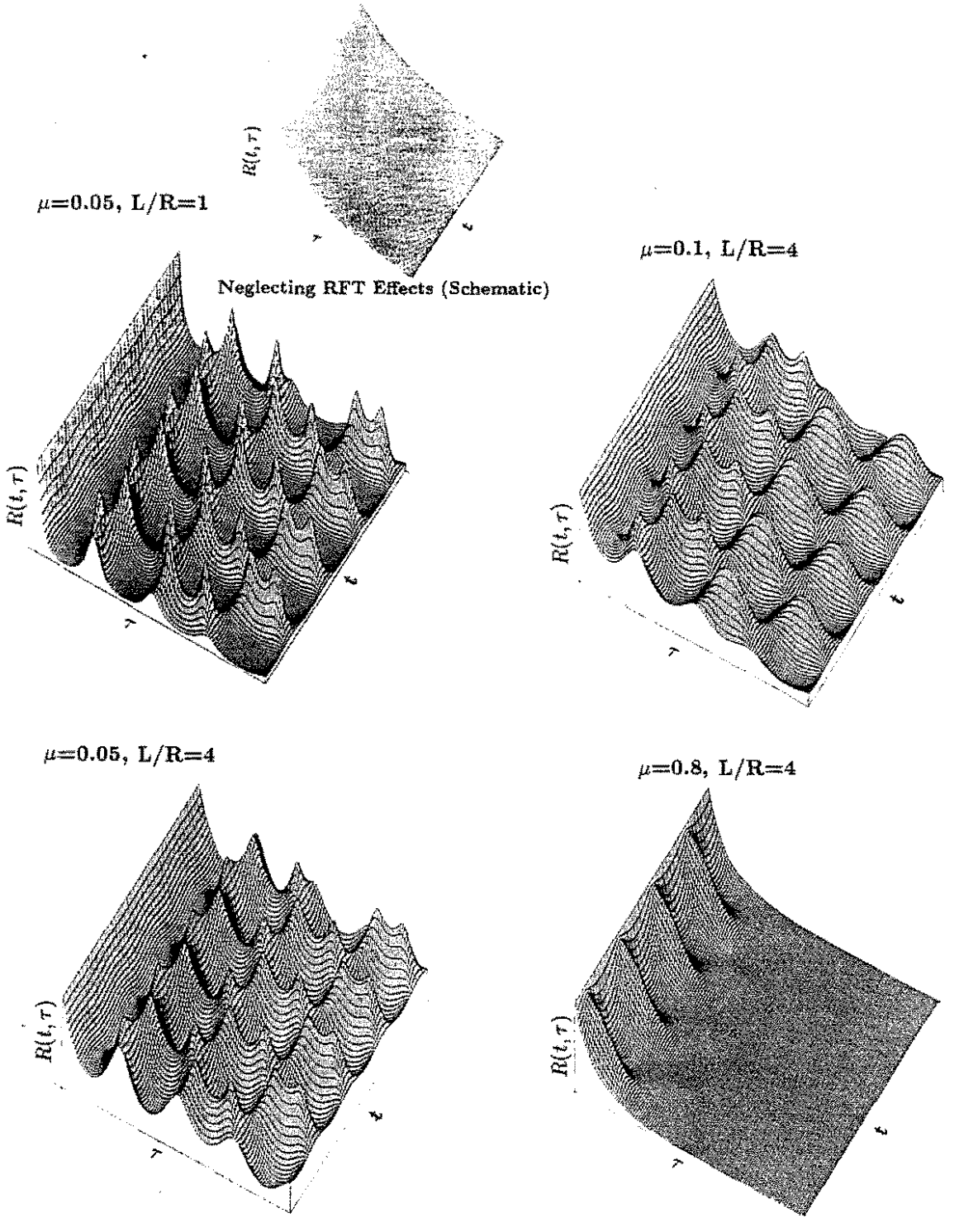

Fig.4 Rotating Frame Turbulence of Exponential Model for different Advance Ratios and Scale length/Rotor Radius Ratios.

The above equation shows that the gust excitation is stationary. The RFT contribution is reflected by the $\sin^2 \tau/2$ term, which introduces the peaks at 1P, 2P etc. in Fig. 2. When the RFT effects are neglected, equation (7a) further simplifies to

$$R_w(\tau) = \sigma_w^2 exp(-b|\tau|) \tag{7b}$$

and the corresponding spectral density function is

$$S_w(f) = \frac{2b}{b^2 + 4\pi^2 f^2} \tag{7c}$$

Frequency-time Spectral Density

The instantaneous or frequency-time spectral density function $S_w(f,t)$ provides a means of describing both the energy transfer with respect to frequency f and the periodically varying nonstationarity with respect to time t. To this end, the autocovariance function $R_w(t,\tau)$ given by equation (5) can be expressed as the inverse Fourier transform of $S_w(f,t)$ (Refs. 15 and 16):

$$R_w(t,\tau) = E\left[w(t-\tau/2)w(t+\tau/2)\right] = \int_{-\infty}^{\infty} S_w(f,t)e^{i2\pi f\tau} df \tag{8a}$$

where E represents the averaging or expectation operation. For τ=0,

$$\sigma_w^2(t) = E\left[w^2(t)\right] = R_w(t,0) = \int_{-\infty}^{\infty} S_w(f,t)dt \geq 0 \tag{8b}$$

Now, from equation (8a),

$$S_w(f,t) = \int_{-\infty}^{\infty} R_w(t,\tau)e^{-i2\pi f\tau} d\tau \tag{8c}$$

Since $R_w(t,\tau)$ given by equation (5) is an even function of τ, the above equation simplifies to

$$S_w(f,t) = \int_{-\infty}^{\infty} R_{xx}(t,\tau)\cos 2\pi f\tau d\tau \tag{8d}$$

Thus $S_w(f,t)$ is real valued, a noteworthy feature. Since the variance $\sigma_w^2(t)$ can be identified as a measure of turbulence energy, the instantaneous spectrum $S_w(f,t)$ in equation (8b) shows the distribution of energy in the (f,t) plane. Further, the $S_w(f,t)$

is physically realizable when compared to the conventional double-frequency spectrum $S_w(f_1, f_2)$, which, having both the real part (co-spectrum) and the imaginary part (quad spectrum), is not physically realizable and has much diminished physical meaning. RFT, along with its energy transfer, represents a complicated phenomenon, and further research is required for a detailed description of $R_w(t, \tau)$, equation (5) and $S_w(f, t)$, equation (8c). Nevertheless a heuristic description, based on the computed $S_w(f, t)$ results as shown in Figs. 5 and 6, is presented here. Fig. 6 presents sections of $S_w(f, t)$ for discrete values of t. As seen from Fig. 5, $S_w(f, t)$ is periodic along the t-axis and decreases rapidly with increasing values of f (Also see $S_w(f, n\pi)$, n=0,1,2,... in Fig. 6). The location of isolated peaks at 1P, 2P etc. is as expected. In fact, $S_w(f, n\pi)$ is identical to the S(f) shown as the upper-left inset in Fig. 2. What is rather unexpected is the occurrence of pairs of peaks around P/2, P, 3P/2 etc. This probably represents the presence of deterministic harmonics modulating the stationary or nonstationary sample functions of w(t). Such harmonics cause displacement of the locations of spectral density peaks along the frequency axis. Another aspect of Fig. 5 that merits further investigation is the abrupt change in $S_w(f, t)$ along the t-axis at discrete locations.

Blade Response Computations

The isolated blade model has first, second and third flap bending modes and uses the ONERA-Peters dynamic stall lift model (Refs.17 and 18). Basically, the treatment refers to a deterministic, linearized system subjected to stationary random excitations without RFT effects and to nonstationary random excitations with RFT effects (Ref.4). Inspite of the simplicity of a linear model with only flap bending degrees of freedom, the model is adequate to demonstrate the RFT effects of energy transfer from the low-frequency to the high-frequency region. For the nonstationary case, the conventional shaping-filter approach is not viable. Therefore, the variance matrix $R_X(t)$ of the state vector X(t) representing flapping deflections, their rates and the dynamic stall states

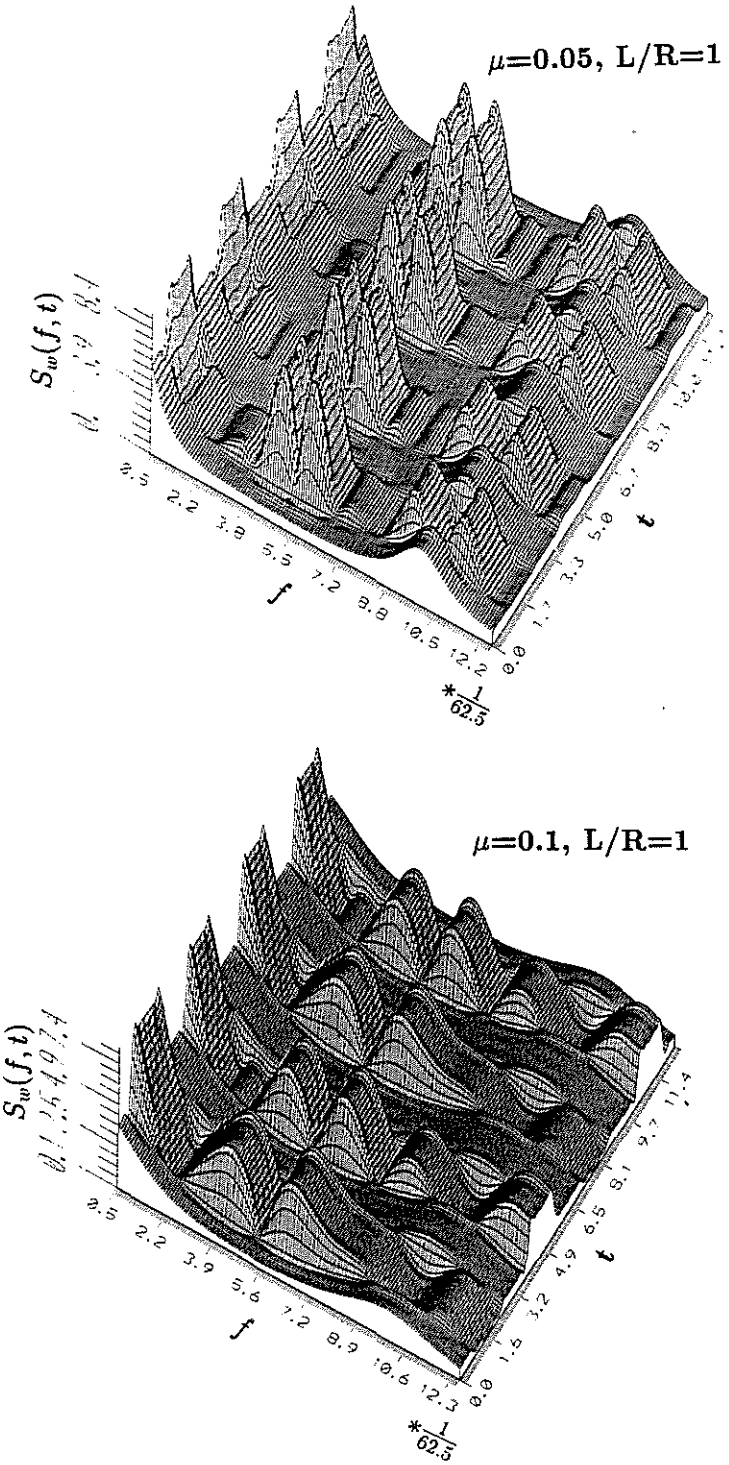

Fig.5 Instantaneous or Frequency-Time Spectra of Exponential Model.

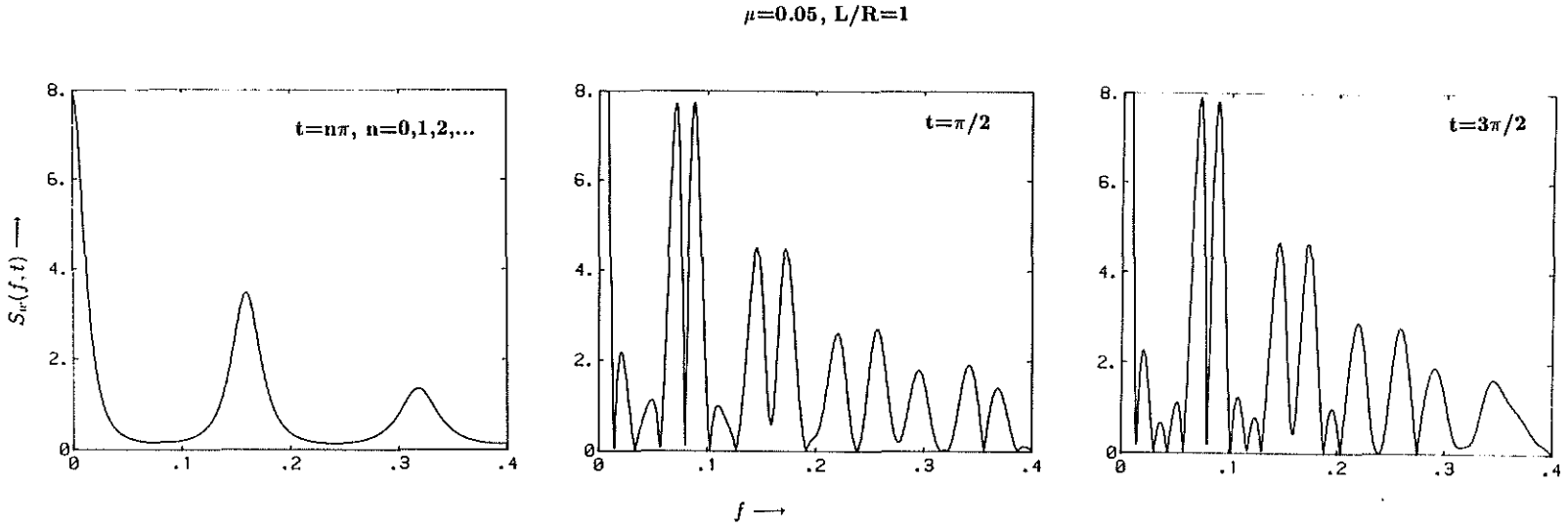

Fig.6 Sections of the Instantaneous Spectrum for Discrete Times.

is computed from the relation:

$$E\left[X(t)X^T(t)\right] = R_X(t) = \int_0^t \int_0^t \Phi(t,\tau_1)R_w(\tau_1,\tau_2)\Phi^T(t,\tau_2)d\tau_1 d\tau_2 \qquad (9)$$

where $\Phi(t,\tau)$ is the state transition matrix.

For the hovering case, the system and the gust excitations both with and without RFT effects are stationary. Therefore, the conventional spectral density approach is much simpler to use, and the results are easy to interpret. With $H(f)$ representing the system frequency response function, and $S_w(f)$ the gust input spectral density function, the response or state spectral density matrix $S_X(f)$ is given by

$$S_X(f) = |H(f)|^2 S_w(f) \qquad (10)$$

In the subsequent discussion of numerical results, equations (7) and (10) are used for the hovering conditions. When the RFT effects are included, the Fourier transform of $R_w(\tau)$ in equation (7a) is computed numerically to obtain the spectral density function $S_w(f)$. When the RFT effects are neglected, the closed-form expression for $S_w(f)$, equation (7c), is used. In forward flight, equation (9) in combination with equation (5) is used for both the without-RFT and with-RFT cases. However, a note of caution is in order. The preceding development, equations (9) and (10) and the threshold-crossing statistics are based on the assumption that the system is mildly nonlinear and that the response variables, flapping deflection and its rate, are jointly Gaussian. This assumption merits further scrutiny , and its validity is not addressed in this preliminary investigation.

Response Statistics

The response statistics are generated for the following base line values: $0 \leq \mu \leq 0.2$, $1 \leq L/R \leq 4$, thrust coefficient=0.006, fundamental flap natural frequency P_1 (made dimensionless by rotational frequency) varying from 1.03 to 1.1 and Lock number γ=8.

Fig. 7 shows the response spectral density of the first flap bending mode as the main figure and those of the second and third flapping modes as inset figures. The results

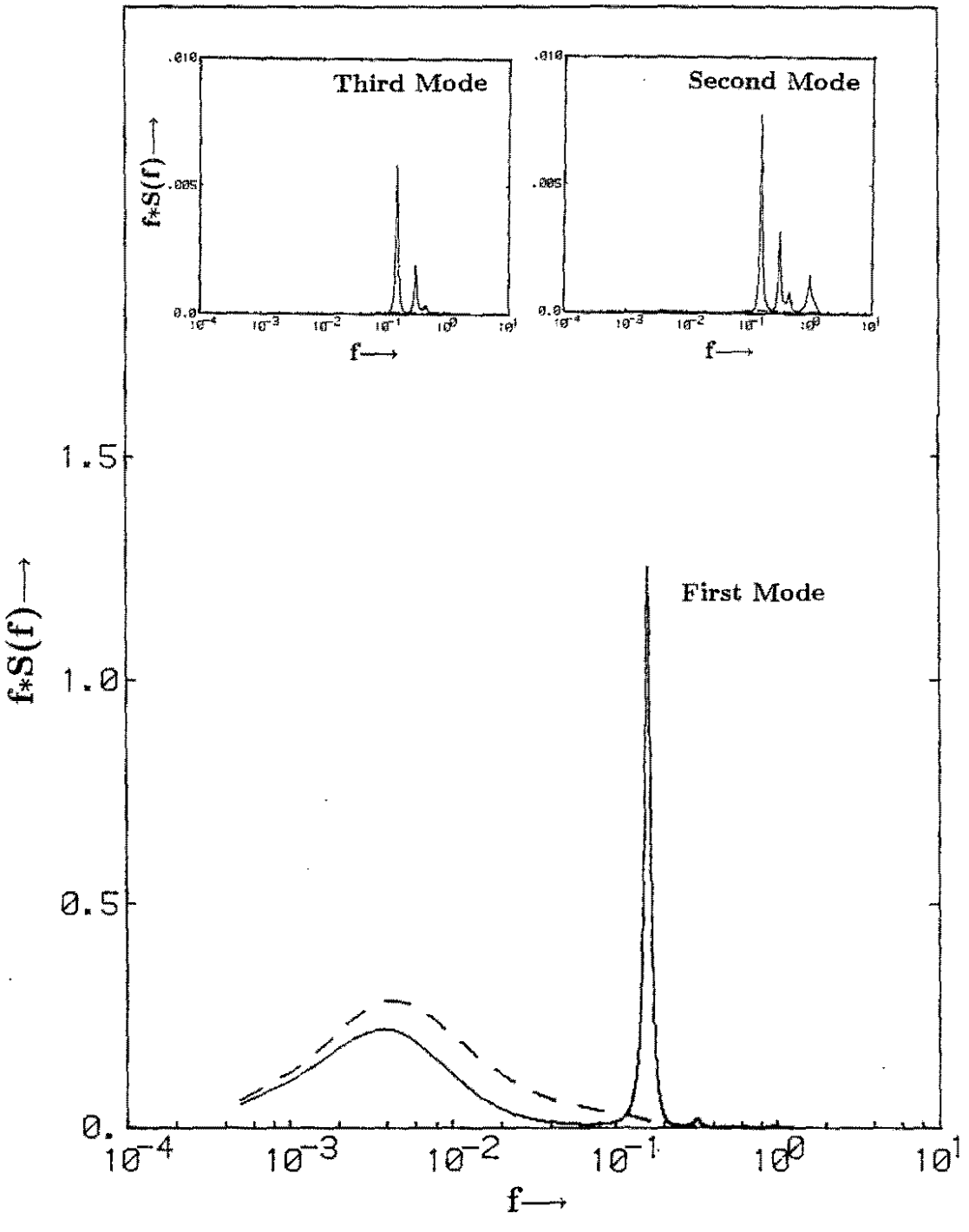

Fig.7 Flapping Response Spectral Densities in Hover

refer to the hovering condition with P_1=1.03 and L/R=4. They are better appreciated in conjunction with Fig. 2, which shows the input spectral density. It is reiterated that the results are presented as f S(f) versus ln f to focus on the impact of energy transfer due to RFT effects from the low-frequency to the high-frequency region. In the low-frequency region, the response spectral density of the first flapping mode with RFT excitation is less than that of the same mode without RFT effects (space-fixed turbulence model). This is because of the energy transfer to the high-frequency region in the RFT description. Thus, in comparison with the response due to RFT excitation, the response due to neglecting RFT effects (space-fixed description) is more severe in this low-frequency region. This is expected because almost all of the turbulence energy in the space-fixed description is concentrated in the low-frequency region (See left inset in Fig. 2). This also explains why the response spectral density rapidly approaches zero with increasing frequency. The effect of transfer of energy to the high-frequency region with a dominant peak at 1P is reflected by the response spectral density due to RFT excitation, which also has a peak close to P_1=1.03. Furthermore, the high-frequency second and third flapping modes are virtually unaffected by the space-fixed turbulence since there is little energy to excite the system at such high frequencies. Though of much smaller magnitude when compared to the first mode spectral density, the RFT does excite the high-frequency modes; the RFT model captures the transfer of energy with peaks at 2P, 3P etc., as shown in Fig. 2. In summary, results of Fig. 7 show that the RFT due to its inherent energy transfer and the occurrence of peaks significantly affects the high-frequency modes and that this impact is virtually suppressed in the space-fixed description.

Figure 8 shows the rms value of the flapping response for μ= 0.1, a low-speed forward-flight condition. While Figs. 8a and 8b show the rigid-blade case respectively for P_1=1.1 and 1.4, Fig. 8c shows the first flap bending mode for P_1=1.1. The rigid blade is not appreciably affected by RFT for realistic values of P_1, which for hingeless rotors is close to 1.1. By comparison, the first flap bending mode rms response, σ_{β_1}, is affected by RFT as shown in Fig. 8c. This is probably due to the coupling effect of the second and third modes, which are high-frequency modes affected by the transfer

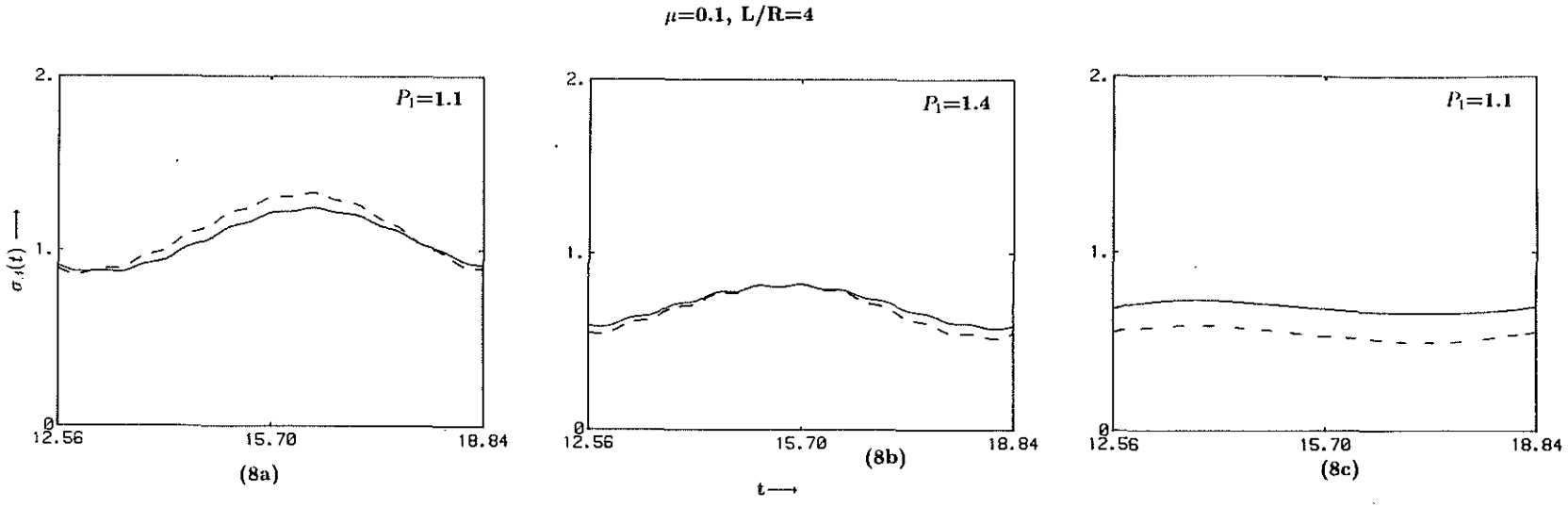

Fig.8 Flapping Response RMS Values (— RFT, ---- Space-fixed)

of turbulence energy to the high-frequency region. For P_1=1.1, the global maximum and the nonstationarity of σ_{β_1} over one rotor revolution are less than those of the corresponding rigid-blade results. These two features of the first flap bending mode rms results vis-a-vis the rigid-blade results are surprising and merit further research.

Finally, Figs. 9 and 10 show the dynamic stall effects on response statistics with RFT effects: the rigid flapping standard deviation $\sigma_\beta(t)$ and the average number of up-crossings of the zero threshold level per unit time, $E\left[N_{+\beta}(\xi,t)\right]$. Such threshold-crossing statistics are required in fatigue and ride-quality studies, and they are used to approximate high-level peak statistics even for processes that are not narrow band (Ref.19). Fig. 9 clearly shows that dynamic stall aggravates gust sensitivity. The expectation of threshold-crossing rate in Fig. 10 shows that the total number of zero-level up-crossings over one rotor revolution (i.e. $\int_0^{2\pi} E\left[N_{+\beta}(0,t)\right] dt$) substantially increases due to dynamic stall effects. However, the instantaneous threshold-crossing pattern qualitatively remains the same with and without RFT effects.

Conclusions

This preliminary study investigates the stochastic structure of RFT and its effects on flap bending response statistics for low-speed conditions and leads to the following conclusions:

1. RFT, or rotating frame turbulence, is the actual turbulence experienced by a blade station and requires noneulerian or moving-frame description. It is (weakly) stationary in hover. In forward flight, it is nonstationary, and though it is periodically stationary, it is not mean square periodic; see equations (5) and (6).

2. The instantaneous or frequency-time spectrum $S_w(f,t)$ provides a feasible approach to predicting the transfer of energy from the low-frequency region to the high-frequency region and the periodically varying nonstationarity.

3. The response statistics comprising spectral density, rms values and threshold-crossing expectation rates are significantly affected by RFT.

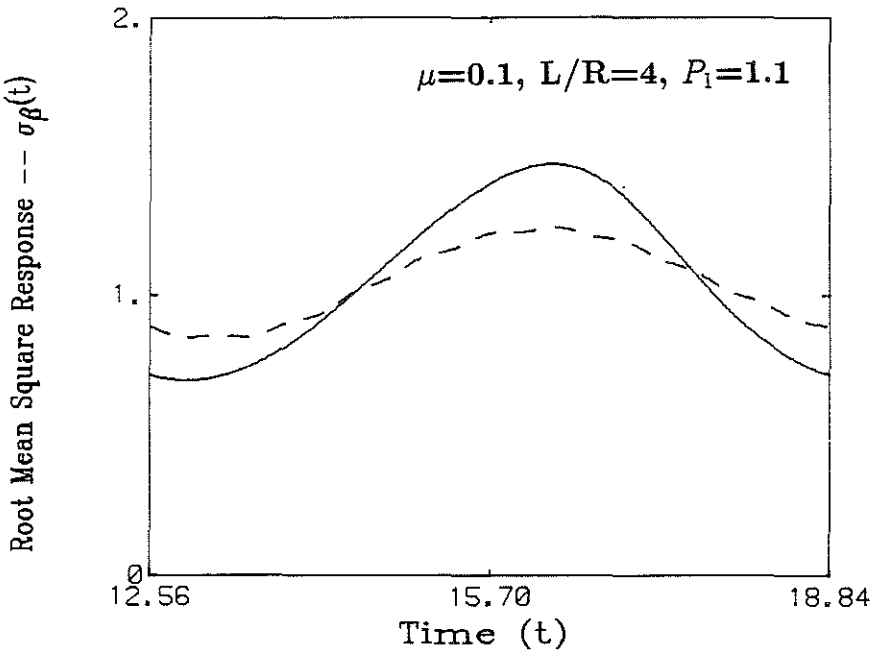

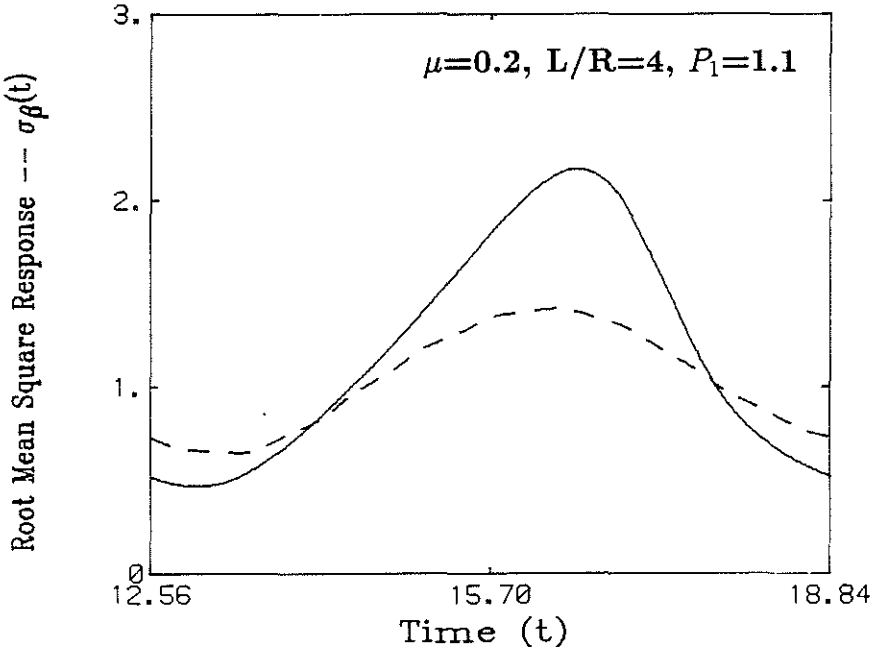

Fig.9 Flapping Response RMS Values
(— with Dynamic Stall,
---without Dynamic Stall).

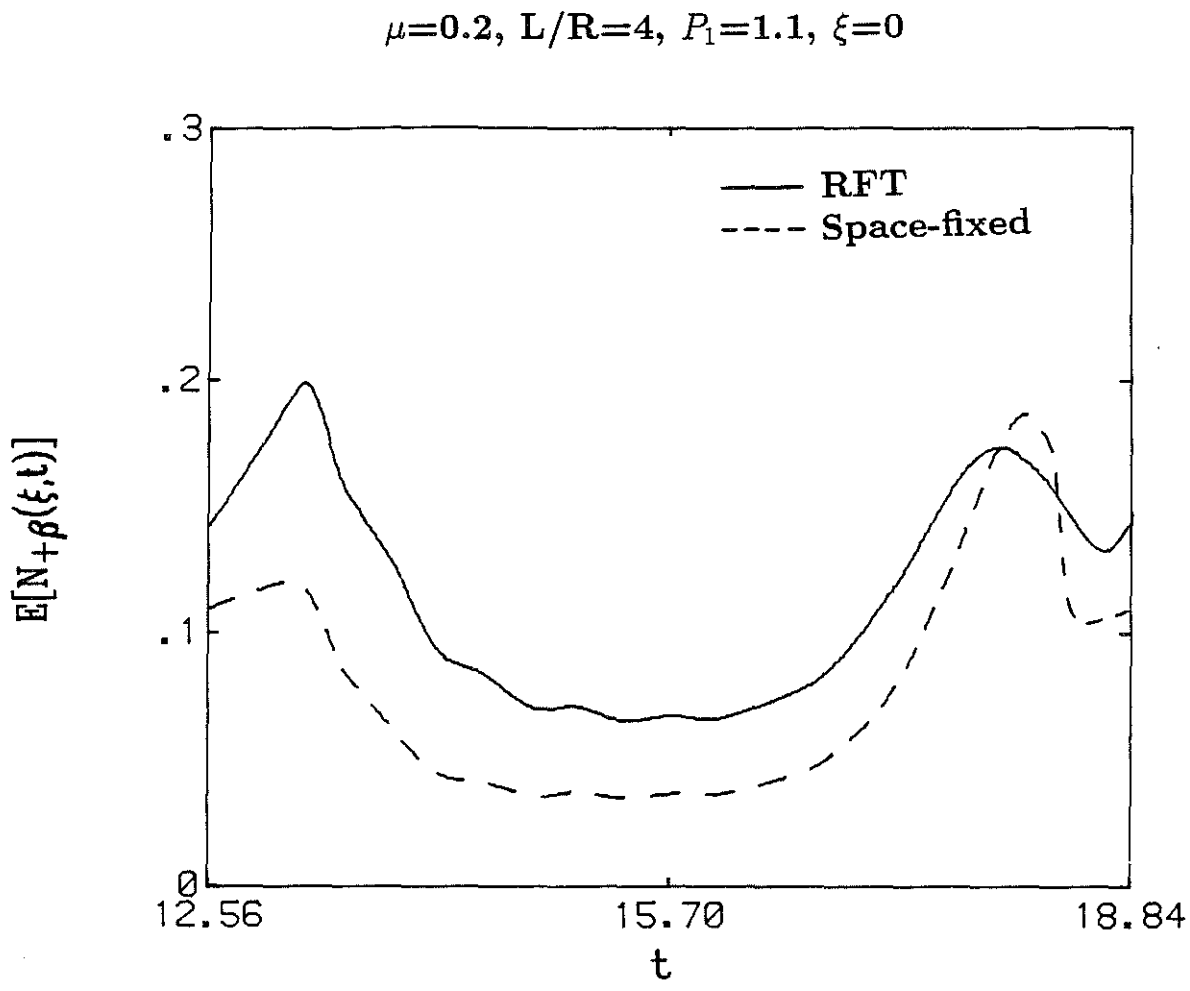

Fig.10 RFT Effects on Threshold-Crossing Expectation Rates with Dynamic Stall.

Acknowledgement

This work is sponsored by the U.S. Army Research Office under grant No. DAAL03 and by the NASA-Ames University Consortium under subcontract No. E-16-606-S1 from the Georgia Institute of Technology. The view, opinion and/or findings contained in this report are those of the authors, and should not be construed as an official Department of the Army position, policy, or decision, unless so designated by other documentation.

References

1. Dahl, H.J. and Faulkner, A.J., "Helicopter Simulation in Atmospheric Turbulence," *Vertica*, Vol.3, (7), April 1978.

2. Carucim, D., McCallum, K. and Higman, J., "Dynamic Interface Flight Test and Simulation Limitations," 11th European Rotorcraft Forum, London, England, September 1985.

3. Schrage, D.P., Prasad, J.V.R. and Gaonkar, G.H., "A Study of the Effects of Rotating Frame Turbulence (RFT) on Helicopter Flight Mechanics," 74 AGARD Symposium of the Flight Mechanics Panel, Gol, Norway, May 1989.

4. Gaonkar, G.H., "Gust Response of Rotor and Propeller Systems," *Journal of Aircraft*, Vol.18, (5), 1981.

5. Ham Norman, D., Wereley Norman, M. and von Ellenrieder Karl. D., "Active Control of Gust and Interference Induced Vibration of Tilt-Rotor Aircraft," American Helicopter Society 45th Annual Forum, Boston, Massachusetts, May 1989.

6. Aiken, E.W., Labacqz, V.J., Chen, R.T.N. and Key, D.L., "Rotorcraft Handling Qualities Design Criteria Development," NASA CP 2495, March 1987.

7. Prussing, J.E. and Lin, Y.K., "A Closed-Form Analysis of Rotor Blade Flap- Lag Stability in Hover and Low-Speed Forward Flight in Turbulent Flow," *Journal of the American Helicopter Society*, July 1983, 28(3), 42-46.

8. Prussing, J.E. and Lin, Y.K., "Rotor Blade Flap-Lag Stability in Turbulent Flows," *Journal of the American Helicopter Society*, April 1982, 27(2), 51-57.

9. Fuh, J.S., Hong, C.Y.R., Lin, Y.K. and Prussing, J.E., "Coupled Flap-Torsional Response of a Rotor Blade in Forward Flight due to Atmospheric Excitations," *Journal of the American Helicopter Society*, July 1983, 28(3), 3-12.

10. Elliot, A.S. and Chopra, I., "Hingeless Rotor Response to Random Gusts in Forward Flight," AIAA Dynamics Specialists Conference, Monterey, California, 1987.

11. Gaonkar, G.H., "Random Vibration Peaks in Rotorcraft and the Effects of Nonuniform Gusts," *Journal of Aircraft*, Vol.14, (7), 1977.

12. Connell, J.R., "The Spectrum of Wind Speed Fluctuations Encountered by a Rotating Blade of Wind Energy Conversion System," *Solar Energy*, Vol.29, (5), 1982.

13. Anderson, M.B. and Fordham, E.J., "An Analysis of Results from an Atmospheric Experiment to Examine the Structure of the Turbulent Wind as seen by a Rotating Observer," University of Cambridge, Cavendish Laboratory, Cambridge, U.K., 1982.

14. Gaonkar, G.H., "A Perspective on Modeling Rotorcraft in Turbulence," *Probabilistic Engineering Mechanics Journal*, Vol.3, (1), 1988.

15. Bendat, J.S. and Piersol, A.G., *Random Data*, John Wiley and Sons, New York, 1986, Chapter 12.

16. Mark, W.D., "Power Spectrum Representation for Nonstationary Random Vibration," *Status and Recent Developments*, Elsevier Publishers, The Netherlands, 1985.

17. Karunamoorthy, S.N., *Use of Hierarchial Elastic Blade Equations for Automatic Trim for Helicopter Vibration Analysis*, Doctor of Science Thesis, Washington University, August 1985.

18. Peters, D.A. and Chouchane, M., "Effect of Dynamic Stall on Helicopter Trim and Flap-Lag Response," *Journal of Fluids and Structures*, Vol.1, 1987.

19. Lin, Y.K., *Probabilistic Theory of Structural Dynamics*, Krieger Publishing Company, Malabar, Florida, 1976, Chapter 9.